



# Plasmon-enhanced photoluminescence from TiO<sub>2</sub> and TeO<sub>2</sub> thin films doped by Eu<sup>3+</sup> for optoelectronic applications

Marcin Łapiński<sup>\*1</sup>, Jakub Czubek<sup>1</sup>, Katarzyna Drozdowska<sup>2</sup>, Anna Synak<sup>3</sup>,  
Wojciech Sadowski<sup>1</sup> and Barbara Kościelna<sup>1</sup>

## Full Research Paper

Open Access

### Address:

<sup>1</sup>Institute of Nanotechnology and Materials Engineering, Gdansk University of Technology, Advanced Materials Center, Gabriela Narutowicza 11/12, 80-233 Gdańsk, Poland, <sup>2</sup>Faculty of Electronics, Telecommunications and Informatics, Digital Technologies Center, Gdansk University of Technology, Gabriela Narutowicza 11/12, 80-233 Gdańsk, Poland and <sup>3</sup>Faculty of Mathematics, Physics and Informatics, University of Gdańsk, Wita Stwosza 57, 80-308 Gdańsk, Poland

### Email:

Marcin Łapiński<sup>\*</sup> - marcin.lapinski@pg.edu.pl

\* Corresponding author

### Keywords:

gold nanostructures; luminescence; plasmon resonance

*Beilstein J. Nanotechnol.* **2021**, *12*, 1271–1278.

<https://doi.org/10.3762/bjnano.12.94>

Received: 30 July 2021

Accepted: 04 November 2021

Published: 22 November 2021

Associate Editor: A. J. Meixner

© 2021 Łapiński et al.; licensee Beilstein-Institut.

License and terms: see end of document.

## Abstract

In this work we study the luminescence properties of europium-doped titanium dioxide and tellurium oxide thin films enhanced by gold plasmonic nanostructures. We propose a new type of plasmon structure with an ultrathin dielectric film between plasmonic platform and luminescent material. Plasmonic platforms were manufactured through thermal annealing of the gold thin film. Thermal dewetting of gold film results in spherical gold nanostructures with average dimensions of 50 nm. Both, luminescent TiO<sub>2</sub>:Eu and TeO<sub>2</sub>:Eu films were deposited by RF magnetron sputtering from mosaic targets. The morphology of the gold nanostructures was investigated by SEM and TEM, while the composition of oxides film was analyzed by XPS. Luminescence properties were studied on the basis of excitation and emission spectra. The experiments show that the additional dielectric layer enhances the luminescence intensity. Such structures could be potential candidates as phosphors in white LEDs.

## Introduction

The rapid development of optoelectronics leads to challenges in the search for new luminescence materials. Especially the fabrication of white LEDs requires more efficient phosphors. Potential new materials can be found through the computation of luminescent thin films and plasmonic platforms. Such a hybrid

structure can be formed by thin oxide layers doped with rare-earth ions deposited on metal nanostructures [1-3]. Plasmonic resonance can be observed in metallic nanostructures, so-called plasmonic platforms, and thin films. Among different plasmonic materials, gold nanostructures exhibit resonance in the

visible range and have been extensively studied as a material for light absorption and emission improvement [4–8]. Titanium dioxide seems to be one of the most popular and widely used oxide material as matrix for rare-earth ions [9–13]. Tellurium dioxide can be also considered as excellent in hosting rare-earth ions because of its low phonon energy (ca. 700–800  $\text{cm}^{-1}$ ), which allows to minimize non-radiative losses [14–16]. Modification of oxide thin films can be implemented in many ways. The change of deposition parameters and working gasses, doping with various elements, or annealing at an elevated temperature are the most commonly used procedures [17,18]. It gives enormous possibilities for manufacturing thin films with novel properties and opens fields of new applications. Especially, doping of oxide materials by rare-earth ions positively influences the luminescent properties. Rare-earths ions represent a vast group of luminescent materials that exhibit light emission in the visible range [19,20]. Among them, europium (Eu) has been intensely studied for a few decades. Although Eu usually assumes a trivalent oxidation state ( $\text{Eu}^{3+}$ ), the divalent state ( $\text{Eu}^{2+}$ ) is also stable, but characterized by different luminescent properties. The  $\text{Eu}^{3+}$  emission spectrum consists of sharp lines, which are ascribed to  ${}^5\text{D}_0 \rightarrow {}^7\text{F}_J$  ( $J = 0\text{--}6$ ) transitions (intra-configurational 4f transitions), observed in the range of 570–840 nm [21–23]. As a red light emitter,  $\text{Eu}^{3+}$  may be employed in various optical devices.

In this work we compare two types of matrix for europium ions, namely titanium dioxide and tellurium dioxide. We show possibilities to enhance the luminescence by plasmon resonance. These nanostructures could find practical applications, for example, as phosphor material in LEDs.

## Experimental

Corning 1737 glass was chosen as a substrate for film deposition. The substrates were gently cleaned with warm acetylacetone, then rinsed in ethanol and dried at 50 °C. Plasmonic nanostructures were prepared by thermal dewetting of gold thin films. Thin Au films with a thickness of 2.8 nm were deposited using a tabletop DC magnetron sputtering coater (EM SCD 500, Leica) in pure Ar plasma (argon, Air Products, 99.999%) at a

pressure of 0.2 Pa. The round Au target with 99.99% purity was sputtered by 30 W of incident power. The rate of Au layer deposition was about 4 Å/s. Thickness was controlled by a built-in quartz crystal microbalance. As prepared films were subsequently put in a hot furnace for the formation of nanostructures. Samples were annealed at 550 °C for 15 min in air atmosphere. The formation of metallic nanostructures has been described in detail in our previous works [24–26]. On the prepared plasmonic platforms a dielectric buffer layer was deposited. We chose two kinds of layers. The first one,  $\text{Al}_2\text{O}_3$ , with different thicknesses in a range of 2 to 8 nm was deposited by atomic layer deposition (ALD) using a Beneq TFS 200 ALD system. This method provides precise control over the thickness with atomic accuracy. Trimethylaluminum (Sigma-Aldrich) and purified water were used as precursors. The deposition of the atomic layers was conducted at 200 °C. The second kind of dielectric layer was  $\text{TiO}_2$ . It was prepared by radio frequency (RF) reactive magnetron sputtering using an Omicron Nanotechnology four targets sputter system. A Ti target (99.9%) was sputtered in an argon–oxygen atmosphere ( $\text{Ar}/\text{O}_2$  flow ratio: 5 sccm:30 sccm, both gasses from Air Products, 99.999%). The used RF power of 60 W resulted in the deposition with a ratio ca. 0.1 Å/s. Luminescent  $\text{TiO}_2\text{:Eu}$  or  $\text{TeO}_2\text{:Eu}$  films were deposited by RF magnetron sputtering. Metallic Ti–Eu (99.9%) or Te–Eu (99.9%) mosaic targets with a diameter of 50.8 mm were sputtered for about 50 min in argon–oxygen atmosphere ( $\text{Ar}/\text{O}_2$  flow ratio: 5 sccm:30 sccm) at a power of 40 W. This resulted in deposited films with a thickness of ca. 300 nm (deposition rate ca. 0.1 Å/s). The deposition process of  $\text{TeO}_2\text{:Eu}$  films was described in our previous work [27]. The preparation of all  $\text{TiO}_2$ ,  $\text{TeO}_2\text{:Eu}$ , and  $\text{TiO}_2\text{:Eu}$  layers was conducted at 200 °C. The pressure in the chamber was approximately 0.2 Pa and the distance between target and substrate was approximately 10 cm. The sputtering system was equipped with a quartz crystal microbalance for the in situ measurements of film thickness. In order to obtain uniform heating of substrates and homogeneous films, a rotation of sample holder equal to 1 rpm was employed. All deposition parameters are collected in Table 1. A schematic view of the prepared samples is presented in Figure 1.

**Table 1:** Magnetron sputtering parameters.

Deposited material	Au	$\text{TiO}_2$	$\text{TiO}_2\text{:Eu}$	$\text{TeO}_2\text{:Eu}$
target	Au	Ti	Te–Eu (mosaic)	Ti–Eu (mosaic)
power supply	DC	RF	RF	RF
power (W)	30	60	40	40
gas composition $\text{Ar}/\text{O}_2$ (sccm)	100:0	5:30	5:30	5:30
working pressure (Pa)	0.2	<0.2	<0.2	<0.2
deposition rate (Å/s)	4	0.1	0.1	0.1

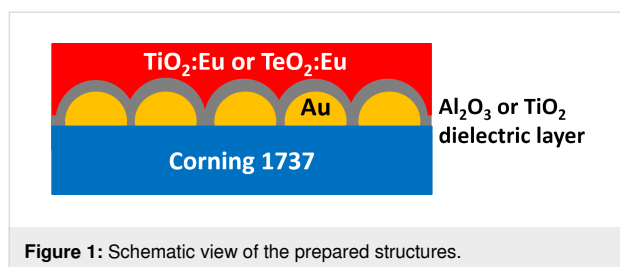


**Figure 1:** Schematic view of the prepared structures.

To analyze the morphology of the plasmonic platforms, a Zeiss CrossBeam 540 scanning electron microscope (SEM) operated at 2 kV was used. For microstructure analysis of the plasmonic structures, a TALOS F200X high-resolution transmission electron microscope (HRTEM) was used. The chemical composition of the luminescent layers was investigated by X-ray photoelectron spectroscopy (XPS). Measurement was performed using Omicron Nanotechnology equipment at room temperature and under ultrahigh vacuum conditions, at a pressure below  $1.1 \times 10^{-6}$  Pa. A Mg K $\alpha$  X-ray source was operated at 15 kV and 300 W. XPS analysis were performed using CASA XPS software package with Shirley background subtraction and the least-square Gaussian–Lorentzian – GL(30) curve fitting algorithm. Calibration of obtained spectra to the binding energy of 285 eV for C 1s was conducted. Additionally, a built-in Ar ion gun was used to etch the surface of the films. To obtain depth profiles of the chemical composition, layers were etched for 2, 6, and 8 min. Optical transmittance spectra of all prepared structures were measured using an Evolution 220 UV–visible spectrophotometer in the range of 200–1000 nm. Luminescence excitation and emission spectra were recorded using a Scinco FluoroMate FS-2 fluorescence spectrometer. Excitation spectra were monitored at the wavelength of  $\lambda_{em} = 615$  nm in a range of 350–460 nm, whereas emission spectra were collected in a range of 560–630 nm with an excitation wavelength of  $\lambda_{exc} = 394$  nm.

## Results and Discussion

### Plasmonic platforms

The quality of the gold plasmonic platforms was examined by SEM and TEM. The SEM image presented in Figure 2a shows a good uniformity of the prepared Au nanostructures. Nanoislands cover the whole substrate surface. Additionally, the HRTEM image of a cross section of a single nanoisland is shown in Figure 2b [25,26]. It can be seen, that the nanostructure with a diameter of ca. 50 nm is not perfectly spherical, but flattened on the substrate side. An exemplary transmittance spectrum recorded for the plasmonic platform is presented in Figure 3. A strong transmittance minimum, corresponding to plasmon resonance is observed at about 530 nm. The rapid decrease of transmittance at 350 nm is caused by absorption of glass substrate and can be noticed for other samples as well.

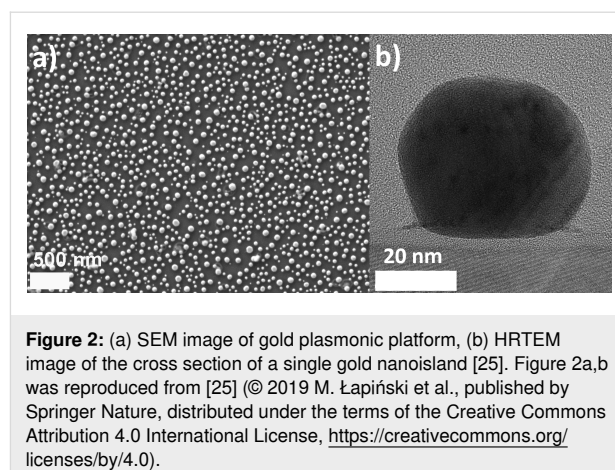


**Figure 2:** (a) SEM image of gold plasmonic platform, (b) HRTEM image of the cross section of a single gold nanoisland [25]. Figure 2a,b was reproduced from [25] © 2019 M. Łapiński et al., published by Springer Nature, distributed under the terms of the Creative Commons Attribution 4.0 International License, <https://creativecommons.org/licenses/by/4.0>.

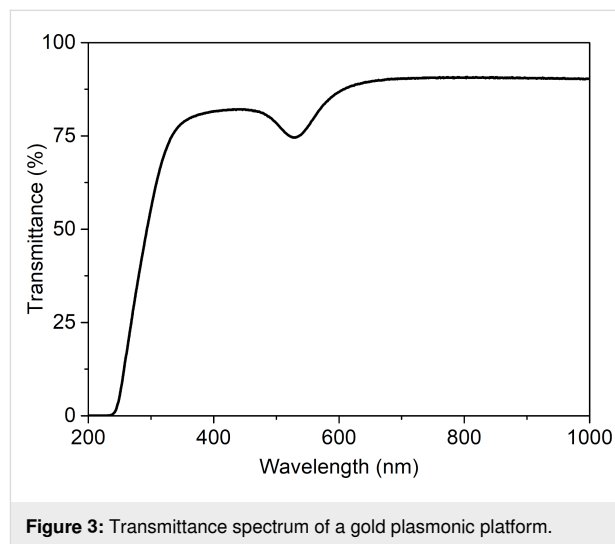


**Figure 3:** Transmittance spectrum of a gold plasmonic platform.

### TiO<sub>2</sub>:Eu-based structures

The chemical composition of the luminescent titanium dioxide doped with europium was examined using XPS. The spectra of Ti 2p and Eu 4d core level electrons are presented in Figure 4. The experimental curve can be deconvoluted in two peaks at 458.2 eV and 463.9 eV, with a splitting energy of 5.7 eV, what is characteristic for Ti<sup>4+</sup> [28–30]. Deconvolution of the Eu 4d spectrum is complicated. As it can be seen in Figure 4, the sample includes both Eu<sup>3+</sup> and Eu<sup>2+</sup> ions [31,32]. The Eu 4d doublet separation was considered as 5.7 eV for Eu<sup>3+</sup> and 5.6 eV for Eu<sup>2+</sup>. The doublet that is assigned to Eu<sup>3+</sup> ions dominates over the Eu<sup>2+</sup> doublet. This led to the conclusion that the quantity of Eu<sup>3+</sup> ions far exceeds that of Eu<sup>2+</sup> ions. The calculated ratio Eu<sup>3+</sup>/Eu<sup>2+</sup> was ca. 90%:10%. Additionally, on the basis of the survey spectrum the total percentage content of europium in the TiO<sub>2</sub>:Eu layer was calculated to be 5%.

Figure 5 shows the UV–vis transmittance spectra for all prepared TiO<sub>2</sub>:Eu structures. It can be seen that the TiO<sub>2</sub>:Eu thin

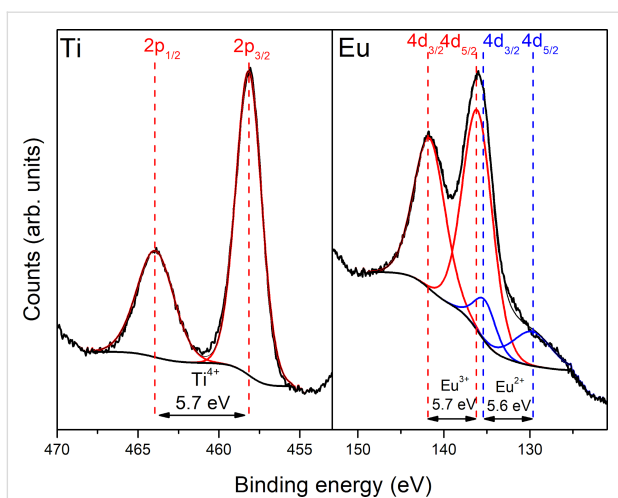


**Figure 4:** XPS spectra of Ti2p and Eu4d spectra of TiO<sub>2</sub>:Eu luminescent film.

film deposited directly on the glass substrate has a flat transmission characteristic with a transmittance of ca. 85%. For the luminescence layer deposited directly on a plasmonic platform, without dielectric film, a transmission minimum at 650 nm is visible. It corresponds to the surface plasmonic resonance effect and is strongly redshifted in comparison to plasmon platform characteristics (Figure 3). This phenomenon is directly related to Mie's theory and can be caused by changes of the electric permittivity over the gold nanostructures [7,8,33]. A shift is also observed in structures with an additional ultrathin Al<sub>2</sub>O<sub>3</sub> film. However, a blueshift occurs here due to the electrical properties of aluminum oxide. Additionally, it can be seen, that the position of the minimum of transmission as function of the Al<sub>2</sub>O<sub>3</sub> film thickness. This may be explained by the different permittivity of the layers [34–36]. Emission and excitation spectra are shown in Figure 6. In the excitation spectrum in the range of 350–460 nm only one peak at 394 nm can be observed. The maximum at that peak corresponds to the <sup>7</sup>F<sub>0</sub>→<sup>5</sup>L<sub>6</sub> electric dipole transition for Eu<sup>3+</sup> [22,37]. The peaks intensities are strongly enhanced when the luminescent layer is deposited on the plasmonic platform with a dielectric Al<sub>2</sub>O<sub>3</sub> layer. The most intense peaks appear for films with 4 and 6 nm thickness. The emission spectra show only one significant peak at 591 nm. It corresponds to the <sup>5</sup>D<sub>0</sub>→<sup>7</sup>F<sub>1</sub> magnetic dipole transition. This type of transition is observed in centrosymmetric structures. This led to the conclusion that there might be some nanocrystal areas in the TiO<sub>2</sub>:Eu films. It is in line with our previous structural investigations. XRD measurements showed an amorphous or nanocrystalline structure of the oxide layers deposited by magnetron sputtering [31]. The intensity of luminescence is enhanced for structures with additional dielectric layer and is the highest for the TiO<sub>2</sub>:Eu layer deposited on plasmonic platforms with 4 or 6 nm of Al<sub>2</sub>O<sub>3</sub>. In contrast, a dielectric layer with a

thickness of 8 nm completely neutralizes the impact of the plasmonic platform. The increase of luminescence for samples with plasmonic nanostructures can be explained by a local concentration of the electric field around the nanostructures. It could increase the rate of excitation [3]. The additional Al<sub>2</sub>O<sub>3</sub> dielectric layer separates plasmonic gold nanostructures and TiO<sub>2</sub>:Eu luminescent film, which changes the conditions of electromagnetic interaction between plasmons and luminescent material.

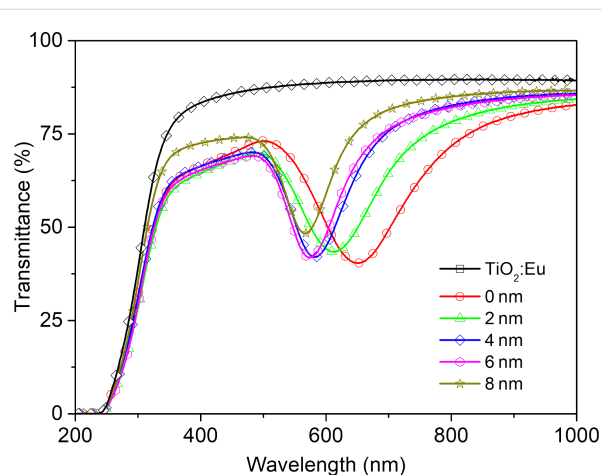


**Figure 5:** UV-vis spectra of a TiO<sub>2</sub>:Eu film and TiO<sub>2</sub>:Eu films deposited on the plasmonic platform without a dielectric layer (0 nm) and with a dielectric Al<sub>2</sub>O<sub>3</sub> layer with different thickness, in a range of 2 to 8 nm.

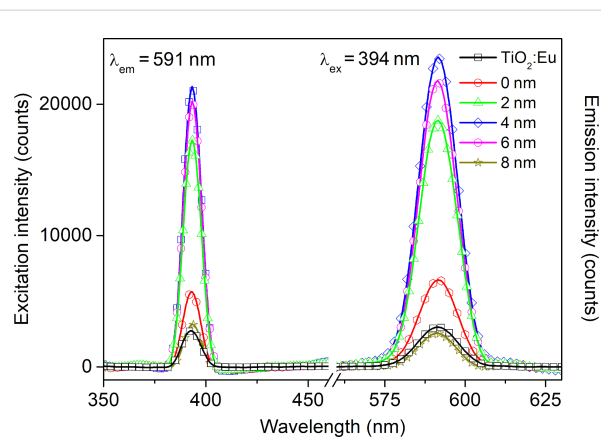


**Figure 6:** Excitation and emission spectra of a TiO<sub>2</sub>:Eu film and TiO<sub>2</sub>:Eu films deposited on the plasmonic platform without a dielectric layer (0 nm) and with a dielectric Al<sub>2</sub>O<sub>3</sub> layer with different thickness, in a range of 2 to 8 nm.

## TeO<sub>2</sub>:Eu-based structures

The results of the XPS analysis of TeO<sub>2</sub>:Eu luminescent layer are presented in Figure 7. Two peaks at 587.3 and 576.07 eV, with an energy separation of 10.37 eV, correspond to tellurium in the fourth valence state (Te<sup>4+</sup>) and are consistent with litera-

ture data [27,38]. The highly oxidative atmosphere during the sputtering process results in a lack of metallic tellurium in the deposited film. The Eu 4d spectrum can be deconvoluted into two doublets, which suggests the presence of europium in two valence states. Lines recorded at 142.36 and 136.76 eV correspond to  $\text{Eu}^{3+}$ , while those observed at 136.40 and 130.90 eV were assigned to  $\text{Eu}^{2+}$ . The energy separation in both doublets equals to 5.60 and 5.50 eV for  $\text{Eu}^{3+}$  and  $\text{Eu}^{2+}$ , respectively, in accordance with literature [31,32]. The  $\text{Eu}^{3+}$  doublet is characterized by greater intensity and dominates over the  $\text{Eu}^{2+}$  lines. For quantitative analysis, integral intensities of europium doublets were compared. The  $\text{Eu}^{3+}/\text{Eu}^{2+}$  ratio was ca. 90%:10%. Total amount of dopant in a sample was calculated to ca. 5%, on the basis of survey spectra. The amount of luminescent dopant in both titanium dioxide and tellurium dioxide matrixes should be sufficient to observe luminescence from the thin films. According to literature, percentage of luminescent ions in the host material should not exceed 10%. Otherwise, emission quenching may occur [39]. Additionally, a depth profile of concentration was measured. XPS results after etching of the  $\text{TeO}_2:\text{Eu}$  film showed good chemical uniformity over the whole thickness of the layer, which is shown in Figure 8. After 8 min of etching the film was completely removed from the Corning glass substrate and no signals from Te 3d and Eu 4d lines were detected.

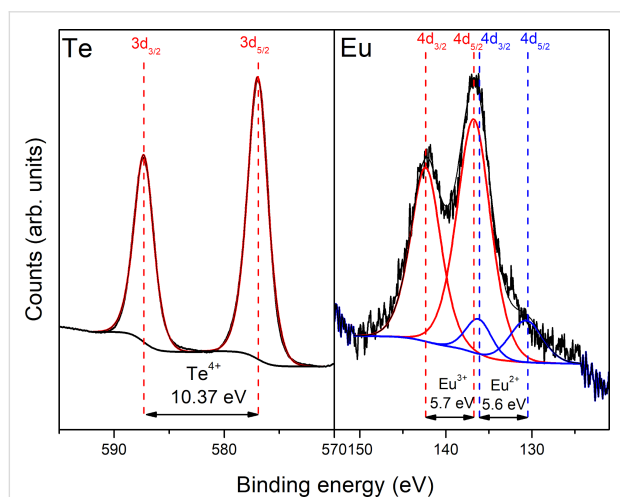


**Figure 7:** XPS spectra of Te 3d and Eu 4d regions of the  $\text{TeO}_2:\text{Eu}$  luminescent layer.

To compare optical properties and investigate the influence of plasmonic resonance on the intensity of luminescence, transmission and luminescence spectra were recorded for the single luminescent oxide layer and the luminescent films deposited on gold nanostructures, in both configurations with and without dielectric  $\text{Al}_2\text{O}_3$  layer. The transmittance spectra in a range of 200–1000 nm are presented in Figure 9. The  $\text{TeO}_2:\text{Eu}$  layer is

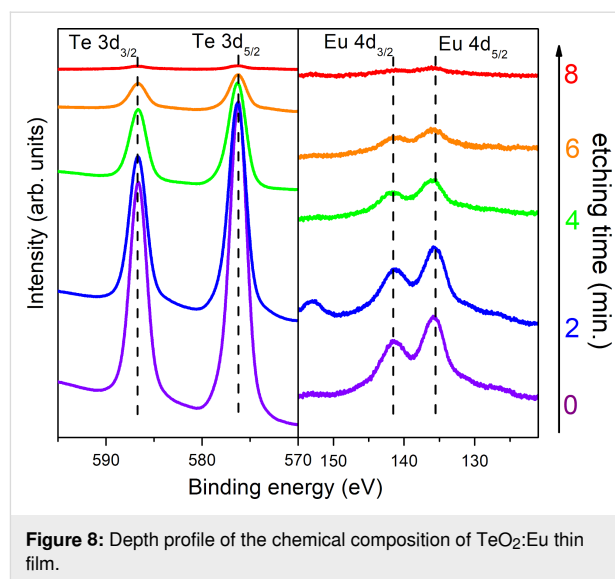


**Figure 8:** Depth profile of the chemical composition of  $\text{TeO}_2:\text{Eu}$  thin film.

characterized by a high transmission intensity with a transmittance of approximately 85% in the visible range. Multilayers with gold nanostructures exhibit a minimum, which is ascribed to plasmonic resonance. The shift of the resonance wavelength in a multilayer, as well as the change of transmission band intensity can be explained by the change of plasmonic platform surrounding. In comparison with air both  $\text{TeO}_2:\text{Eu}$  and  $\text{Al}_2\text{O}_3$  layers exhibit a much greater permittivity, which affects the optical properties of plasmonic nanostructures and redshifts the resonance wavelength [34,35,40,41]. The excitation and emission spectra samples are shown in Figure 10. One main spectral line can be distinguished on excitation spectra for all samples. It is positioned at 394 nm and corresponds to the  ${}^7\text{F}_0 \rightarrow {}^5\text{L}_6$  transition in  $\text{Eu}^{3+}$ . As far as absorption and excitation of  $\text{Eu}^{3+}$  ions are concerned, it is the most probable and most frequently observed transition according to literature [23,42,43]. Samples deposited on Au plasmonic platforms show an increased intensity of the excitation peak. Moreover, samples with an additional aluminium oxide ultrathin film exhibit a higher excitation intensity. The increased excitation for samples with Au nanostructures may be ascribed to the plasmonic resonance effect, which results in greater absorption of light and, consequently, more efficient excitation of the luminescent material. The changing of the surrounding of plasmonic structures has visible impact on the luminescent properties of a sample. The redshift of the resonance wavelength and the decrease of transmittance observed in Figure 9 caused by  $\text{Al}_2\text{O}_3$  may successfully tune the optical properties of gold plasmonic nanostructures to obtain a more efficient excitation of the luminescent layer with europium ions. The characteristic narrow emission band at 591 nm was assigned to the  ${}^5\text{D}_0 \rightarrow {}^7\text{F}_1$  magnetic dipole transition in  $\text{Eu}^{3+}$  [40,41]. Its intensity is higher for samples with Au platforms than for the reference sample ( $\text{TeO}_2:\text{Eu}$ ) and reaches



the greatest value for 4 nm of  $\text{Al}_2\text{O}_3$  layer. In general, greater excitation of luminescent material leads to more efficient emission. The observed magnetic dipole transition is characteristic for a uniform distribution of luminescent ions in a host matrix. Usually, such centrosymmetric matrices are crystalline structures or consist of some crystal areas. The intensity of excitation and emission peaks for titanium dioxide- and tellurium dioxide-based structures, are presented in Figure 11. The luminescence intensity and the influence of the plasmonic platform for both kinds of phosphors is comparable.

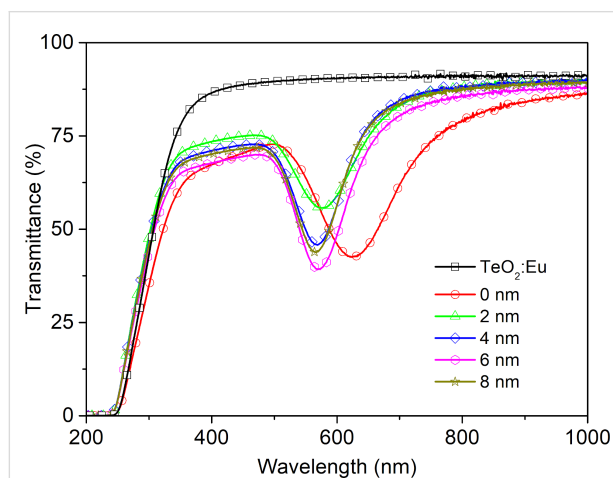


**Figure 9:** UV-vis spectra of a  $\text{TeO}_2:\text{Eu}$  film and  $\text{TeO}_2:\text{Eu}$  films deposited on the plasmonic platform without a dielectric layer (0 nm) and with a dielectric  $\text{Al}_2\text{O}_3$  layer with different thickness, in a range of 2 to 8 nm.

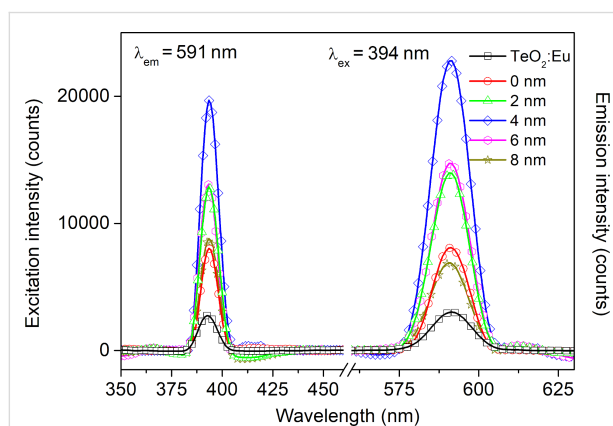


**Figure 10:** Excitation and emission spectra of  $\text{TeO}:\text{Eu}$ -based structures.

Additionally, we decided to change the dielectric layer from  $\text{Al}_2\text{O}_3$  to  $\text{TiO}_2$ . It enabled the production of structures in a one-step process during the deposition of multilayers by magnetron sputtering. On the basis of emission spectra for structures with alumina oxide, 4 nm of titanium dioxide was selected as a

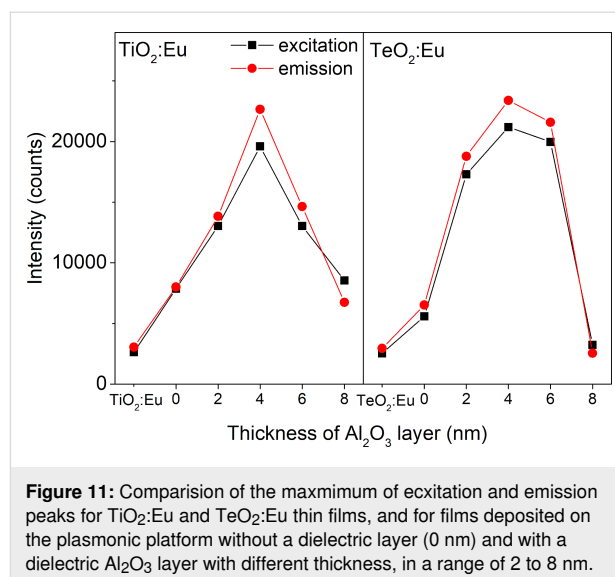


**Figure 11:** Comparison of the maximum of excitation and emission peaks for  $\text{TiO}_2:\text{Eu}$  and  $\text{TeO}_2:\text{Eu}$  thin films, and for films deposited on the plasmonic platform without a dielectric layer (0 nm) and with a dielectric  $\text{Al}_2\text{O}_3$  layer with different thickness, in a range of 2 to 8 nm.

dielectric layer. The optical characteristics are presented in Figure 12 and Figure 13. Because of the different dielectric constants of both types of dielectric layers, a shift of plasmon resonance position is observed (Figure 12). From the luminescence spectra in Figure 13 it can be seen that it is possible to enhance of luminescence intensity by an ultrathin  $\text{TiO}_2$  film, almost as much as by  $\text{Al}_2\text{O}_3$ .

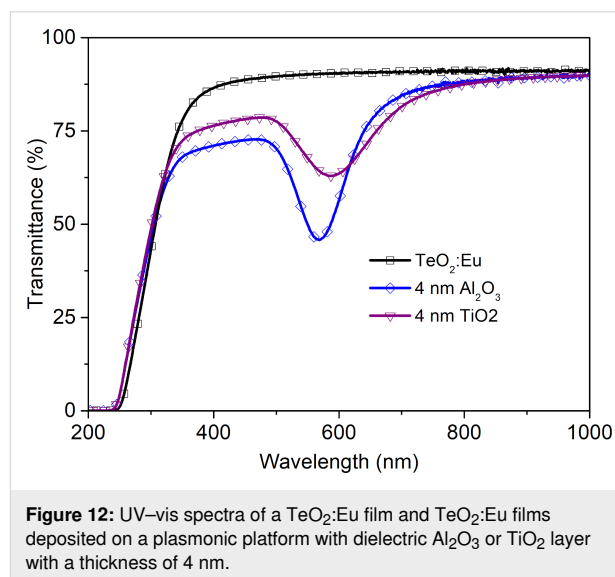


**Figure 12:** UV-vis spectra of a  $\text{TeO}_2:\text{Eu}$  film and  $\text{TeO}_2:\text{Eu}$  films deposited on a plasmonic platform with dielectric  $\text{Al}_2\text{O}_3$  or  $\text{TiO}_2$  layer with a thickness of 4 nm.

## Conclusion

In this work we showed an interesting material in which europium ions dispersed in a thin  $\text{TiO}_2$  or  $\text{TeO}_2$  film are responsible for the emission of light. The intensity of the luminescence can be enhanced by the plasmon resonance from Au nanostructures. The gain is tunable by the thickness of a  $\text{Al}_2\text{O}_3$  thin film deposited as a separator between metallic nanostruc-

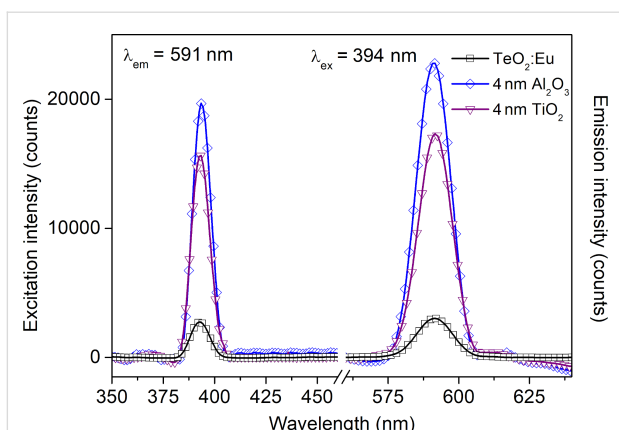


**Figure 13:** Excitation and emission spectra of a TeO<sub>2</sub>:Eu film and TeO<sub>2</sub>:Eu films deposited on a plasmonic platform with dielectric Al<sub>2</sub>O<sub>3</sub> or TiO<sub>2</sub> layer with a thickness of 4 nm.

tures and the luminescent layer. Interestingly, no transition caused by the electric dipole (615 nm, typical for Eu<sup>3+</sup> ions) was observed in the emission spectrum for both kinds of metal oxide matrix. The main emission peak corresponds to the transition occurring via magnetic dipole, which is independent of the host matrix. Such a phenomenon usually takes place in materials in which Eu<sup>3+</sup> ions are located at sites with higher symmetry, and explaining this behavior in the presented samples would require further research. Anyway, we believe that the presented structures could be attractive for optoelectronic applications.

## ORCID® IDs

Marcin Łapiński - <https://orcid.org/0000-0002-3283-2886>

Jakub Czubek - <https://orcid.org/0000-0001-6694-9073>

Katarzyna Drozdowska - <https://orcid.org/0000-0003-0056-0967>

Anna Synak - <https://orcid.org/0000-0001-8264-7833>

Wojciech Sadowski - <https://orcid.org/0000-0002-1229-3723>

Barbara Kościelska - <https://orcid.org/0000-0002-9352-9581>

## References

- Ashok, A.; Arackal, A.; Jacob, G. *Nanosci. Nanotechnol. (Rosemead, CA, U. S.)* **2015**, *5*, 71–81.
- Maier, S. A. *Plasmonics: Fundamentals and Applications*; Springer US: New York, NY, 2007. doi:10.1007/0-387-37825-1
- Łapiński, M.; Synak, A.; Gapska, A.; Bojarski, P.; Sadowski, W.; Kościelska, B. *Opt. Mater. (Amsterdam, Neth.)* **2018**, *83*, 225–228. doi:10.1016/j.optmat.2018.05.002
- Korzeb, K. Electronic Materials. In *Overview of fabrication methods of plasmonic materials and selected alternative materials for plasmonic applications*; Gajc, M.; Pawlak, D., Eds.; ITME: Warszawa, 2014; Vol. 42, pp 18–29. <https://rcin.org.pl/dlibra/publication/72835/edition/53503/content>
- Hutter, E.; Fendler, J. H. *Adv. Mater. (Weinheim, Ger.)* **2004**, *16*, 1685–1706. doi:10.1002/adma.200400271
- Matsishin, M. J.; Kucherov, A. I.; Ushenin, I. V.; Lyapin, A. M.; Lopatynskiy, A. M.; Chegel, V. I.; Rachkov, A. E. *Biopolym. Cell* **2017**, *33*, 268–281. doi:10.7124/bc.000959
- Cheng, Z.; Li, G.; Liu, M. *Sens. Actuators, B* **2015**, *212*, 495–504. doi:10.1016/j.snb.2015.02.050
- Krajczewski, J.; Kołataj, K.; Kudelski, A. *RSC Adv.* **2017**, *7*, 17559–17576. doi:10.1039/c7ra01034f
- Domaradzki, J.; Kaczmarek, D.; Prociów, E.; Wojcieszak, D.; Sieradzka, K.; Mazur, M.; Lapinski, M. *Opt. Appl.* **2009**, *39*, 815–823.
- Wojcieszak, D. *Appl. Surf. Sci.* **2017**, *421*, 128–133. doi:10.1016/j.apsusc.2017.01.040
- Conde-Gallardo, A.; Garcia-Rocha, M.; Palomino-Merino, R.; Velásquez-Quesada, M. P.; Hernández-Calderón, I. *Appl. Surf. Sci.* **2003**, *212–213*, 583–588. doi:10.1016/s0169-4332(03)00131-4
- Leostean, C.; Stefan, M.; Pana, O.; Cadis, A. I.; Suci, R. C.; Silipas, T. D.; Gautron, E. *J. Alloys Compd.* **2013**, *575*, 29–39. doi:10.1016/j.jallcom.2013.04.067
- Peng, A.; Xie, E.; Jia, C.; Jiang, R.; Lin, H. *Mater. Lett.* **2005**, *59*, 3866–3869. doi:10.1016/j.matlet.2005.07.028
- Chopra, N.; Kaur, S.; Kaur, M.; Singla, S.; Marwaha, R.; Sharma, G.; Heer, M. S. *Phys. Status Solidi A* **2018**, *215*, 1700934. doi:10.1002/pssa.201700934
- Fares, H.; Jlassi, I.; Hraiech, S.; Elhouichet, H.; Férid, M. *J. Quant. Spectrosc. Radiat. Transfer* **2014**, *147*, 224–232. doi:10.1016/j.jqsrt.2014.05.029
- Gupta, G.; Balaji, S.; Biswas, K.; Annapurna, K. *AIP Adv.* **2019**, *9*, 045201. doi:10.1063/1.5054190
- Won, D.-J.; Wang, C.-H.; Jang, H.-K.; Choi, D.-J. *Appl. Phys. A: Mater. Sci. Process.* **2001**, *73*, 595–600. doi:10.1007/s003390100804
- Hou, Y.-Q.; Zhuang, D.-M.; Zhang, G.; Zhao, M.; Wu, M.-S. *Appl. Surf. Sci.* **2003**, *218*, 98–106. doi:10.1016/s0169-4332(03)00569-5
- Lucas, J.; Lucas, P.; Le Mercier, T.; Rollat, A.; Davenport, W. *Rare Earths*; Elsevier: Amsterdam, Netherlands, 2015. doi:10.1016/c2012-0-02577-x
- Bai, G.; Tsang, M.-K.; Hao, J. *Adv. Funct. Mater.* **2016**, *26*, 6330–6350. doi:10.1002/adfm.201602142
- Cornejo, C. R. *Luminescence in Rare Earth Ion-Doped Oxide Compounds; Luminescence - An Outlook on the Phenomena and their Applications*; InTech: Rijeka, Croatia, 2016. doi:10.5772/65185
- Binnemans, K. *Coord. Chem. Rev.* **2015**, *295*, 1–45. doi:10.1016/j.ccr.2015.02.015
- Yu, C.; Yang, Z.; Huang, A.; Chai, Z.; Qiu, J.; Song, Z.; Zhou, D. *J. Non-Cryst. Solids* **2017**, *457*, 1–8. doi:10.1016/j.jnoncrysol.2016.11.025
- Kozioł, R.; Łapiński, M.; Syty, P.; Koszelow, D.; Sadowski, W.; Sienkiewicz, J. E.; Kościelska, B. *Beilstein J. Nanotechnol.* **2020**, *11*, 494–507. doi:10.3762/bjnano.11.40
- Łapiński, M.; Kozioł, R.; Cymann, A.; Sadowski, W.; Kościelska, B. *Plasmonics* **2020**, *15*, 101–107. doi:10.1007/s11468-019-01021-9
- Gapska, A.; Łapiński, M.; Syty, P.; Sadowski, W.; Sienkiewicz, J. E.; Kościelska, B. *Beilstein J. Nanotechnol.* **2018**, *9*, 2599–2608. doi:10.3762/bjnano.9.241
- Łapiński, M.; Walas, M.; Gapska, A.; Kulik, D.; Szmytko, A.; Twardowski, P.; Sadowski, W.; Kościelska, B. *Thin Solid Films* **2019**, *691*, 137592. doi:10.1016/j.tsf.2019.137592

28. Kubala-Kukuś, A.; Banaś, D.; Stabrawa, I.; Szary, K.; Sobota, D.; Majewska, U.; Wudarczyk-Moćko, J.; Braziewicz, J.; Pajek, M. *Spectrochim. Acta, Part B* **2018**, *145*, 43–50. doi:10.1016/j.sab.2018.03.012
29. Greczynski, G.; Hultman, L. *Prog. Mater. Sci.* **2020**, *107*, 100591. doi:10.1016/j.pmatsci.2019.100591
30. Desai, N. D.; Khot, K. V.; Dongale, T.; Musselman, K. P.; Bhosale, P. N. *J. Alloys Compd.* **2019**, *790*, 1001–1013. doi:10.1016/j.jallcom.2019.03.246
31. Cho, E.-J.; Oh, S.-J. *Phys. Rev. B* **1999**, *59*, R15613–R15616. doi:10.1103/physrevb.59.r15613
32. Kumar, S.; Prakash, R.; Choudhary, R. J.; Phase, D. M. *Mater. Res. Bull.* **2015**, *70*, 392–396. doi:10.1016/j.materresbull.2015.05.007
33. Garcia, M. A. *J. Phys. D: Appl. Phys.* **2011**, *44*, 283001. doi:10.1088/0022-3727/44/28/283001
34. Barbos, C.; Blanc-Pelissier, D.; Fave, A.; Blanquet, E.; Crisci, A.; Fourmond, E.; Albertini, D.; Sabac, A.; Ayadi, K.; Girard, P.; Lemiti, M. *Energy Procedia* **2015**, *77*, 558–564. doi:10.1016/j.egypro.2015.07.080
35. Aguilar-Gama, M. T.; Ramírez-Morales, E.; Montiel-González, Z.; Mendoza-Galván, A.; Sotelo-Lerma, M.; Nair, P. K.; Hu, H. *J. Mater. Sci.: Mater. Electron.* **2015**, *26*, 5546–5552. doi:10.1007/s10854-014-2111-z
36. Chiu, R.-L.; Chang, P.-H. *J. Mater. Sci. Lett.* **1997**, *16*, 174–178. doi:10.1023/a:1018518832762
37. Walsh, B. M. Judd-Ofelt theory: principles and practices. In *Advances in Spectroscopy for Lasers and Sensing*; Di Bartolo, B.; Forte, O., Eds.; Springer: Dordrecht, 2006; pp 403–433. doi:10.1007/1-4020-4789-4\_21
38. Briggs, D. X-ray photoelectron spectroscopy (XPS). In *Handbook of Adhesion*, 2nd ed.; Packham, D. E., Ed.; John Wiley & Sons, Ltd: Chichester, United Kingdom, 2005; pp 621–622. doi:10.1002/0470014229.ch22
39. Ronda, C. R. Emission and Excitation Mechanisms of Phosphors. In *Luminescence. From Theory to Applications*; Ronda, C., Ed.; Wiley-VCH Verlag GmbH: Weinheim, Germany, 2007; pp 1–34. doi:10.1002/9783527621064.ch1
40. Li, Y.; Fan, W.; Sun, H.; Cheng, X.; Li, P.; Zhao, X. *J. Appl. Phys.* **2010**, *107*, 093506. doi:10.1063/1.3406135
41. Jha, A.; Richards, B. D. O.; Jose, G.; Toney Fernandez, T.; Hill, C. J.; Lousteau, J.; Joshi, P. *Int. Mater. Rev.* **2012**, *57*, 357–382. doi:10.1179/1743280412y.0000000005
42. Đorđević, V.; Miličević, B.; Dramićanin, M. D. Rare Earth-Doped Anatase TiO<sub>2</sub> Nanoparticles. In *Titanium Dioxide*; Janus, M., Ed.; IntechOpen: Rijeka, Croatia, 2017. doi:10.5772/intechopen.68882
43. Li, H.; Zheng, K.; Sheng, Y.; Song, Y.; Zhang, H.; Huang, J.; Huo, Q.; Zou, H. *Opt. Laser Technol.* **2013**, *49*, 33–37. doi:10.1016/j.optlastec.2012.12.007

## License and Terms

This is an Open Access article under the terms of the Creative Commons Attribution License (<https://creativecommons.org/licenses/by/4.0>). Please note that the reuse, redistribution and reproduction in particular requires that the author(s) and source are credited and that individual graphics may be subject to special legal provisions.

The license is subject to the *Beilstein Journal of Nanotechnology* terms and conditions: (<https://www.beilstein-journals.org/bjnano/terms>)

The definitive version of this article is the electronic one which can be found at: <https://doi.org/10.3762/bjnano.12.94>